Materials Science & Engineering C 112 (2020) 110938

Contents lists available at ScienceDirect

Materials Science & Engineering C

journal homepage: www.elsevier.com/locate/msec

Endothelial dysfunction induced by hydroxyl radicals – the hidden face of biodegradable Fe-based materials for coronary stents

E. Scarcello[a,*], I. Lobysheva[b], C. Bouzin[c], P.J. Jacques[d], D. Lison[a], C. Dessy[b]

[a] Université catholique de Louvain, Louvain Centre for Toxicology and Applied Pharmacology, Avenue Hippocrate 57, 1200 Brussels, Belgium
[b] Université catholique de Louvain, Pole of Pharmacology and Therapeutics, Avenue Hippocrate 57, 1200 Brussels, Belgium
[c] Université catholique de Louvain, IREC Imaging Platform, Avenue Hippocrate 55, 1200 Brussels, Belgium
[d] Université catholique de Louvain, Institute of Mechanics, Materials and Civil Engineering, Place Sainte Barbe 2, Louvain-la-Neuve B-1348, Belgium

ARTICLE INFO

Keywords:
Endothelial dysfunction
Biocorrosion
Oxidative stress
Nitric oxide
Reactive oxygen species
Coronary stent

ABSTRACT

Fe-based materials are currently considered for manufacturing biodegradable coronary stents. Here we show that Fe has a strong potential to generate hydroxyl radicals (HO·) during corrosion. This HO· generation, but not corrosion, can be inhibited by catalase. Oxidative stress was observed (increased *HO-1* expression) in aortic rings after direct exposure to Fe, but not in the presence of catalase or after indirect exposure. This oxidative stress response induced an uncoupling of eNOS in, and a consequent reduced NO production by endothelial cells exposed to Fe. In isolated rat aortic rings NO production was also reduced by HO· generated during Fe corrosion, as indicated by the protective role of catalase. Finally, all these mechanisms contributed to impaired endothelium-dependent relaxation in aortic rings caused by HO· generated during the direct contact with Fe.

This deleterious impact of Fe corrosion on the endothelial function should be integrated when considering the use of biodegradable Fe-based alloys for vascular implants.

1. Introduction

During the last decade, biodegradable materials have been developed and investigated as alternatives to permanent implants, notably for cardiovascular stents [1]. The most favorable and suitable coronary stent should, indeed, maintain its mechanical integrity only for the first 6–12 months, and be totally degraded after 12–24 months to avoid chronic inflammation, long-term restenosis or late thrombosis [2]. An ideal biodegradable material for coronary stents should, therefore, demonstrate a perfect compromise between rapid degradation in the body and appropriate mechanical performances. Recently, biodegradable metals were considered as interesting materials because of their good mechanical properties with a specific strength similar to current austenitic stainless steels 316L or Co—Cr alloys [3]. Among them, Fe-based alloys were investigated because they combine relatively high strength, high elastic modulus and high ductility needed for the implantation of a stent [4].

The electrochemical processes that occur at the metallic surface after stenting have a strong effect on the local biological system [5]. Indeed, immediately after implantation of a Fe-based stent, dissolved oxygen drives metal corrosion, generating Fe^{2+} ions and hydrogen peroxide which, together, participate to the Fenton/Haber-Weiss reactions at the surface of the materials thereby generating HO· radicals (Figure 1) [6].

At neutral pH, the main source of HO· implicates the formation of superoxide anion ($O_2\cdot^-$) and is described by the Fenton reaction, which involves a series of one-electron transfer reactions [7]:

$$Fe(0) \rightarrow Fe^{2+} + 2e^- \quad (1)$$

$$Fe^{2+} + O_2 \rightarrow Fe^{3+} + O_2\cdot^- \quad (2)$$

$$Fe^{2+} + O_2\cdot^- \xrightarrow{2H^+} Fe^{3+} + H_2O_2 \quad (3)$$

$$Fe^{2+} + H_2O_2 \rightarrow Fe^{3+} + OH^- + HO\cdot \quad (4)$$

Or by the Haber-Weiss cycle, which includes a two-step reaction [5]:

$$Fe^{3+} + O_2\cdot^- \rightarrow Fe^{2+} + O_2 \quad (5)$$

$$Fe^{2+} + H_2O_2 \rightarrow Fe^{3+} + OH^- + HO\cdot \quad (6)$$

HO· is the most damaging reactive oxygen species (ROS). It is one of the most potent oxidizing agents highly reacting with all biological macromolecules and with significant pro-inflammatory properties [8]. These ROS generated at the implant metal surface can thus affect adjacent cells, such as endothelial or smooth muscle cells. Moreover, these

* Corresponding author.
E-mail address: eleonora.scarcello@uclouvain.be (E. Scarcello).

https://doi.org/10.1016/j.msec.2020.110938
Received 27 May 2019; Received in revised form 14 February 2020; Accepted 5 April 2020
Available online 07 April 2020
0928-4931/

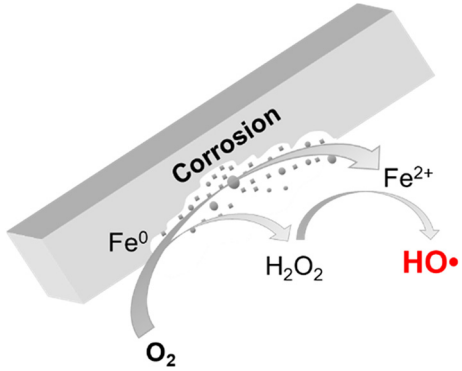

Fig. 1. Simplified mechanism of HO· production from the corrosion of Fe-based materials. HO· is generated via a Fenton reaction driven by Fe^{2+} ions and H_2O_2 jointly produced during the corrosion of Fe^0.

ROS may also be generated by mononuclear phagocytic cells. Indeed, the interactions between metals and the body are controlled by immune cells [5]. Defense cells such as neutrophils can activate NADPH oxidase, bound in both phagosomes and extracellular membranes, to produce ROS in order to attack foreign bodies [9]. NADPH oxidation and the electrons transfer across the membrane reduces oxygen to superoxide anion ($O_2\cdot^-$), which can form hydrogen peroxide (H_2O_2) via the SOD activity. H_2O_2 formed can generate the HO· via the Fenton/Haber-Weiss reactions described above, increasing the corrosion of the material.

These two important sources of ROS represent, therefore, a new paradigm in the interactions between the metallic biomaterial and the corrosion, supporting that corrosion causes biology and biology causes corrosion [5].

Previous experimental investigations on the biocompatibility of metallic materials did not record local or systemic toxicity [10] but the function of the arterial tissue was not assessed. While it is well established in the field of inhalation toxicology that metals can release ROS, including HO· [11], this aspect has not been much explored in the field of biodegradable materials for medical devices [12]. Specifically for Fe-based materials, the possible role of HO· generated by the corrosion deserves a specific attention. Moreover, the possible role of HO· in local tissue response appears very relevant for coronary stents because of the critical role of oxidative stress in the pathogenesis of atheromatous disease. In addition, balloon angioplasty and coronary stent implantation are associated with increased generation of ROS related to alter endothelial and smooth muscle cells [13]. Because corrosion is expected to occur during the whole lifetime of the implant, HO· is expected to be continuously formed at the implant surface, possibly resulting into prolonged inflammation, unsuccessful healing of the surrounding tissues, and/or endothelial dysfunction.

Several studies have emphasized the pivotal role of endothelial dysfunction in the development, progression or clinical complications of atherosclerosis. Although the endothelium plays multiple functions, a reduced vasodilatory response is an indicator of endothelial dysfunction resulting from an unbalance between the production and release of endothelial relaxing (nitric oxide (NO), endothelium-derived hyperpolarizing factor (EDH(F)) and prostacyclin (PGI_2)) and contracting factors (endothelin-1 (ET-1), thromboxane A2 (TxA_2) and prostaglandins (PGs)) [14]. Nitric oxide is known to be one of the most potent vasorelaxant molecule and is produced by endothelial nitric oxide synthase (eNOS) from L-arginine [15]. Reduced NO bioavailability due to decreased eNOS activity and/or ROS-promoted degradation epitomize endothelial dysfunction, setting up the ground for further vascular damages. Here, we hypothesized that HO· accompanying the corrosion of Fe have deleterious impacts on endothelial function. We developed a new *ex-vivo* model using aortic rings to measure endothelial function after exposure to Fe.

2. Materials & methods

2.1. Metallic materials

Fe wire (diameter 0.5 mm) with a purity ≥99.9% and carbonyl Fe powder (size 5–9 μm) with a purity > 99.5% were purchased from Sigma-Aldrich (St Louis, MO). The stainless steel 316L alloy (FeCr18Ni10Mo3) wire (diameter 0.5 mm) was from Goodfellow (Coraopolis, PA). The 316L powder was obtained from gas atomization of commercial bars, 15 mm in diameter, of 316L stainless steel grade. Induction drip-melting of these bars was used to melt the alloy. The liquid was then atomized with high pressure Ar. The resulting powder was then sieved in 3 steps. The first one removed particles > 120 μm. Sieving down to 70 μm and then 20 μm was then carried out. The purity of the 316L powder was verified by inductively coupled plasma - optical emission spectrometry (ICP-OES, Agilent Technologies 5100) analysis (Fe 67.5%, Cr 16.9%, Ni 10.9%, Mo 2.13%, Mn 1.59%).

2.2. Aortic rings

Wistar rats (220 to 250 g) were obtained from the local breeding facility (Animalerie Centrale, Université catholique de Louvain, Brussels, Belgium). All experimental procedures and protocols were approved by the local Ethics Committee « Comité d'Ethique pour l'Expérimentation animale », Secteur des Sciences de la Santé, Université catholique de Louvain, according to National Care Regulation and Directive 2010/63/EU of European Parliament and of the Council. Only male rats were used in this study to avoid hormonal confounding, as estrogens can modulate endothelial function through regulation of the NOS/NO pathway [16].

Rats were anesthetized with an i.p. injection of sodium pentobarbital (90 mg). The descending thoracic (endothelium-dependent relaxation experiments and immunohistochemistry) and/or abdominal (*HO-1* and NO experiments) aorta was dissected over 5 to 6 cm and immediately placed in 5 ml of cold Tyrode buffer with the following composition (mM): NaCl 120.0; KCl 5.9; $CaCl_2$ 2.5; $MgCl_2$ 1.2; Na_2HPO_4. $2H_2O$ 1.2; $NaHCO_3$ 25.0; glucose 11.5. The connective tissue, fat and blood clots were carefully removed from the vessel. All dissection procedures were carefully done to protect the endothelium from damage. The aortic segment was cut with a sterile scissor into 2 to 3 mm rings for the following tests.

2.3. Endothelium contact model

In order to mimic the contact between the endothelium and Fe-based material, we designed a new *ex-vivo* model. A Fe or 316L wire was carefully inserted into the lumen of a vessel ring and placed into a 6-well plate (Greiner Bio-One, Vilvoorde, Belgium) with 10 ml of Tyrode buffer/well. The plate was placed into a water-bath at 37 °C with carbogen (5% CO_2 and 95% O_2) bubbling into the buffer (Photo 1). After 6 h, the wire was carefully removed and the aortic ring was used for subsequent measurements.

Indirect exposure was included as a control to isolate the potential role of solubilized Fe ions by incubating aortic rings with a Fe wire outside the lumen (Photo 2). In some tests, the antioxidant catalase (Sigma-Aldrich, St Louis, MO) was added to the Tyrode buffer at a final concentration of 1000 U/ml.

The surface morphology of Fe and 316L stainless steel wires before and after corrosion was characterized by scanning electron microscopy (SEM Ultra 55®, Zeiss, Oberkochen, Germany) analyses.

2.4. Fluorimetric measurement of hydroxyl radicals

The terephthalate assay is a fluorimetric method to quantify short-lived HO· generated by the material. Disodium terephthalate reacts with HO· leading to the formation of 2-hydroxyterephthalate, a

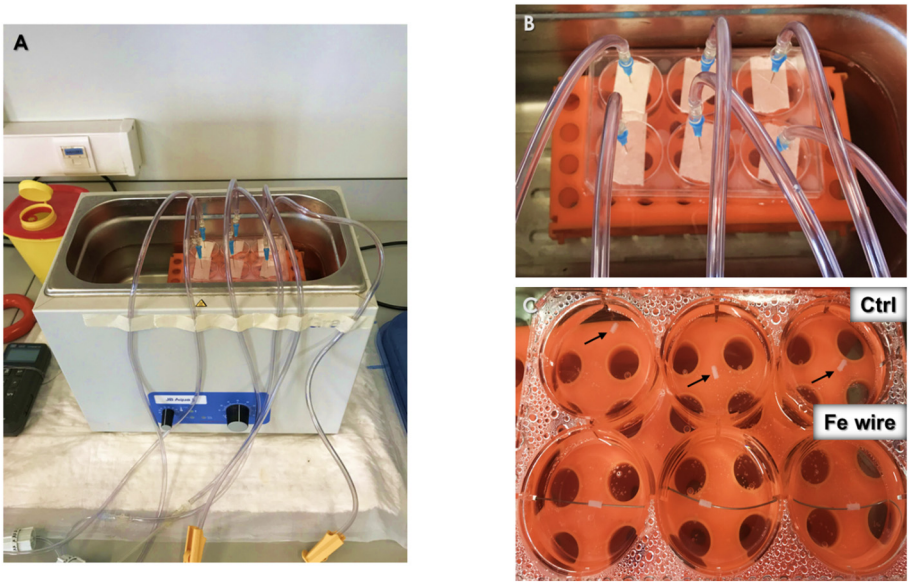

Photo 1. Endothelium-stent contact model. (A, B) 6-well plate in the water-bath at 37 °C with carbogen bubbling. (C) Control rat aortic rings (arrows) vs. aortic rings exposed to Fe wire.

Photo 2. Rat aortic rings (arrows) directly or indirectly exposed to Fe wire.

fluorescent molecule. Disodium terephthalate (99%, Alfa Aesar, Tewksbury, MA) was dissolved in 0.01 M PBS (pH 7.4, Life Technologies, Carlsbad, CA) at a final concentration of 10 mM [17]. Wire samples were washed in absolute ethanol, dried, and immediately suspended in 5 ml of terephthalate solution and incubated for 30 min at 25 °C under continuous stirring. In some assays, the antioxidant catalase (1000 U/ml) was added to the reaction. After incubation, the suspensions were filtered on cellulose acetate membrane (0.22 μm) and the fluorescence of the filtrate was measured on a SpectraMax i3x Multi-Mode microplate reader (Molecular Devices, San Jose, CA) at λ_{ex} = 324 nm and at λ_{em} = 425 nm.

2.5. Immunofluorescence

After exposure to Fe or 316L wire (see Section 2.3), aortic rings were opened and preserved in paraformaldehyde (PFA) 4% for 1 h at 4 °C. Rings were then washed twice in Tris Buffered Saline (TBS)/Triton 0.1% and blocked with 5% bovine serum albumin (BSA) for 1 h. Subsequently, samples were incubated with BMS158 Rabbit Anti-VE-cadherin (Bender Medsystems #BMS158, 1:100 dilution) overnight at 4 °C. After four washing steps, vessel rings were then incubated with Alexa Fluor 568 Donkey Anti-Rabbit (Life Technologies, Carlsbad, CA, 1:200 dilution) overnight at 4 °C. Samples were then washed four times and post-fixed in PFA 4% for 10 min at 4 °C. Incubation with secondary antibodies alone was used as a negative control. Full thickness tissue was mounted in Dako Fluorescence Mounting Medium (Agilent, Santa Clara, CA) and the endothelial surface of the aortic wall examined by structured illumination fluorescence microscopy (Carl Zeiss AxioImager.z1 equipped with an ApoTome.z1 module, Jena, Germany).

2.6. Gene expression experiments

Transcripts of the heme oxygenase-1 (*HO-1*) gene were measured to document oxidative stress in aortic abdominal rings. Rings were directly exposed to Fe wire in the absence/presence of catalase (1000 U/ml), to 316L wire or indirectly as described above. Immediately after exposure, rings were immersed in 1 ml of TriPure Isolation Reagent with 3–4 zirconium beads and disrupted by a multi-directional movement of the tubes at 5000 rpm (Precellys, Montigny-le-Bretonneux, France). Homogenates were recovered and RNA extracted with the TriPure Isolation Reagent (Roche, Mannheim, Germany) according to the manufacturer's protocol, followed by DNase treatment (Invitrogen Inc., Camarillo, CA). RNA was reverse transcribed with M-MLV-Reverse Transcriptase (Invitrogen, Carlsbad, CA) with 700 pmol/μl random hexamers (Eurogentec, Seraing, Belgium) in a final volume of 25.0 μl. The resulting complementary DNA was then diluted 10-fold in sterile UltraPure® water (Invitrogen) and used as template in subsequent real-time polymerase chain reactions (RT-qPCR). Amplified DNA fragments from Human Umbilical Vein Endothelial Cells (HUVECs) exposed to 5.0 μM of Sodium (meta)arsenite (Merck, Saint Louis, MO) were purified and quantified from a 1.5% agarose gel with Nucleospin Extract (Macherey-Nagel, Düren, Germany) and then serially diluted to serve as standards in real-time PCR. Five microliters of diluted cDNA or standards were amplified using SYBR Green technology in a total volume of 20.0 μl on a StepOnePlus™ Real-Time PCR System Thermal Cycling Block (Applied Biosystems, Foster City, CA) according to the following program: 10 min 95 °C and 40 cycles of (15 s 95 °C + 1 min 60 °C). After amplification, a melting curve was generated and data analysis was performed with the StepOne™ Software v2.3 (Applied Biosystems, Thermo Fisher Scientific, Waltham, MA). Primers for *HO-1* and *β-actin* were purchased from Invitrogen Inc.

HO-1: (sense) 5′ GACAGCATGTCCCAGGATTTGT 3′
(antisense) 5′ TTAAAGCCTTCCCTGGACACCT 3′.
β-actin: (sense) 5′ CCCGTGCTGCTGACCGG 3′
(antisense) 5′ CGTCACCGGAGTCCATCAC 3′;

Results were calculated as a ratio of *HO-1* expression (number of copies/ml) to the expression of the reference gene, *β-actin*.

2.7. Nitric oxide measurement by in situ EPR spectroscopy

NO bioavailability was assayed by Electron Paramagnetic

Resonance (EPR) spectroscopy in isolated thoracic aortic rings after Fe or 316L wire exposure with or without catalase as described above. EPR spin trapping measures the concentration of paramagnetic NO adduct accumulated in the aortic rings after stimulation by a Ca(II) ionophore (ionomycin, 5 μM) at 37 °C during 30 min (with or without L-NAME, 2 mM) in the presence of a spin trap (colloid form of [Fe(II)-$(DETC)_2$], 0.5 mM in KREBS buffer) [14]. The composition of the KREBS buffer was: NaCl 99.00 mmol/L, KCl 4.69 mmol/L, KH_2PO_4 1.03 mmol/L, $MgSO_4$ 1.20 mmol/L, $NaHCO_3$ 25.00 mmol/L, glucose 5.00 mmol/L, HEPES 20.00 mmol/L, and $CaCl_2$ 2.00 mmol/L. The EPR spectra were recorded on a X-band EPR spectrometer (MS400, Magnettech, Berlin, Germany). The NO adduct [$NO-Fe(DETC)_2$] exhibits an intense three-line signal. The Magnettech software was used to measure the intensity of the EPR signal of the formed paramagnetic [(DETC)2-Fe(II)-NO] complexes (g1 = 2.035; A_N = 1.3 mT). The intensity of the third hyperfine structure (hfs) signal component was used to characterize the NO production in the aortic rings after normalization [18]. The instrument settings were as follows: modulation frequency, 100 KHz; microwave frequency, 9.35 GHz; microwave power, 20 mW; modulation amplitude, 5G; B_0-field, 330.9438 mT; range, 14.7923 mT; 7 scans. The signal was normalized to the weight of dried aortic rings. All products were purchased from Sigma (Saint Luis, MO).

2.8. Cell culture and exposure

Bovine Aortic Endothelial Cells (BAECs) were purchased from Clonetics (Lonza Group Ltd., Switzerland). Cells were cultured on 0.2% gelatin-coated P100 Petri dishes (Greiner Bio-One) using DMEM (Life Technologies) supplemented with 10% FBS and 100 U penicillin/100 μg streptomycin, and maintained in a humidified incubator (New Brunswick Galaxy® 170S) containing 5% CO_2 at 37 °C. Cells were grown to confluency and harvested by trypsinization. In order to maintain phenotypic characteristics of endothelial cells, a maximum of 8 passages was used. Cells were also routinely tested for the absence of Mycoplasma infection (PCR Mycoplasma Test Kit I/RT, PromoKine, Huissen, the Netherlands). Endothelial cells were plated into P60 or P100 Petri dishes (Greiner Bio-One) and exposed to sterile Fe particles. The particles were freshly suspended in cell culture medium at a stock concentration of 5 mg/ml. Immediately before cell exposure, the particle suspension was diluted to 100 μg/ml (final concentration) in culture medium and vortexed.

2.9. Nitric oxide measurement on cells

Electron Paramagnetic Resonance (EPR) spectroscopy was used to detect NO production by BAECs through the reaction of NO with the spin trap [Fe(II)$(diethyldithiocarbamate)_2$]. In brief, 24 h after exposure to non-cytotoxic doses of the metal (100 μg/ml), endothelial cells were washed with HBSS (Hank's Balanced Salt Solution, Thermo Fisher Scientific, Waltham, MA) twice, treated with or without L-NAME (2.5 mM) and incubated for 30 min at 37 °C in KREBS buffer containing 0.2% BSA. Cells were then treated for 45 min at 37 °C with 0.5 mM of $[diethyldithiocarbamate]_2$-Fe(II) colloid complex in presence (or not) of the Ca(II) ionophore (A23187, 2 μM, Sigma-Aldrich). Cells were then scraped, and frozen in calibrated tubes. The EPR signals were recorded on a X-band EPR spectrometer (MS400, Magnettech, Berlin, Germany) with following EPR parameters: microwave frequency, 9.35 GHz; modulation frequency, 100 kHz; microwave power, 20 mW; modulation amplitude, 5G; time constant, 80 ms; 7 scans; 77 K and analyzed as described above [19]. The signal was normalized to mg of proteins.

2.10. eNOS monomer/dimer and Nrf2 assay

Endothelial cells were exposed to non-cytotoxic doses of Fe (100 μg/ml) with/without catalase (1000 U/ml) and after 24 h, collected and lysed in ice-cold buffer (composition in mM: Tris-HCl 50, pH 8; NaCl 180; EDTA 0.5; NP40 0.2%; phenylmethylsulfonyl fluoride 100) containing a protease inhibitor cocktail (1%; Sigma, Saint Luis, MO). A bicinchoninic acid (BCA) protein assay kit (Pierce, Thermo Scientific) was used to determine the protein concentration of each sample according to the manufacturer's protocol. 15 μg of proteins were loaded per Western blot well, and the migration was performed at 4 °C (eNOS) or 25 °C (*Nrf2*) in non-reducing migration buffer (Tris-EDTA, SDS, glycine) under a voltage of 140 V. After migration, proteins were transferred onto a nitrocellulose membrane with constant amperage of 350 mA for 2 h at 4 °C (transfer buffer: Tris-base, glycine) or RT. The membranes were then incubated in a blocking solution containing Tween 0.1% and BSA 5% for 1 h at RT. For the immuno-detection of the targeted proteins, membranes were incubated with a primary anti-eNOS/NOS Type III antibody (Ab) (250 μg/ml; BD Biosciences, 610297), anti-Nrf2 (D1Z9C) XP® Rabbit (mAb) (250 μg/ml; Cell Signaling Technology, 12721) or anti-HSP90 (250 μg/ml, BD Biosciences, 610419) overnight at 4 °C in Tween/BSA 1%. Membranes were washed in TBS-Tween and incubated with the peroxidase-conjugated secondary antibody for 1 h at RT, washed again and developed by enhanced chemiluminescence (ECL, Amersham) on CL-Xposure film (Thermo Scientific) in the dark room. Films were scanned, and protein bands were quantified by densitometry (ImageJ software, National Institutes of Health). Results were expressed as a ratio of monomeric/monomeric + dimeric eNOS. HSP90 was used as loading control.

2.11. Organ-bath method

After Fe exposure, aortic rings were suspended horizontally between 2 platinium hooks in organ baths filled with 12 ml of Tyrode solution continuously gassed with 95% O2 and 5% CO2 at 37 °C. One stirrup was connected to a displacement device, which allows the investigator to manually adjust the tension of the vessel, and the other one was connected to a force transducer. The contractile tension of the aortic ring was monitored by a force transducer and recorded on data acquisition hardware and software (Powerlab16/35, Labchart8 (ADInstruments). The solution in the chamber was changed every 15 min. Rings were allowed to equilibrate for 90 min under 2 g of resting tension. Total endothelium-dependent relaxation was measured on phenylephrine (Phe; 3 μM) pre-constricted vessels by addition of cumulative doses of carbachol (Cch; 0.1 to 30 μM). NO-dependent relaxation was measured on vessels pretreated in the presence of COX inhibition, indomethacin (INDO; 10 μM), and contracted by depolarization with a high-KCl solution. EDH(F)-mediated relaxation was evaluated in presence of N-Ω-286 Nitro-L-arginine methyl ester (L-NAME; 100 μM), a NOS inhibitor, and INDO on vessels pre-contracted with Phe; finally, PGI2-dependent relaxation was assessed in presence of L-NAME after KCl pre-contraction.

2.12. Statistical analyses

All experiments were repeated at least 3 times. Values are presented as means ± standard error of the mean (S.E.M.) of independent experiments (N) conducted in replicates (n). The data were analyzed with GraphPad Prism (GraphPad software, La Jolla, CA). Differences between groups were analyzed by one-way analysis of variance (ANOVA) test followed by a post-hoc Dunnett's or Tukey's comparison. $p < 0.05$ was considered statistically significant and is indicated with an asterisk or with different superscript letters. $p < 0.01$ compared to the control is indicated with three asterisks.

3. Results

3.1. Fe corrosion generates hydroxyl radicals

Our first goal was to document the ability of Fe wire to generate HO· in aqueous conditions. A Fe wire was incubated in Tyrode buffer

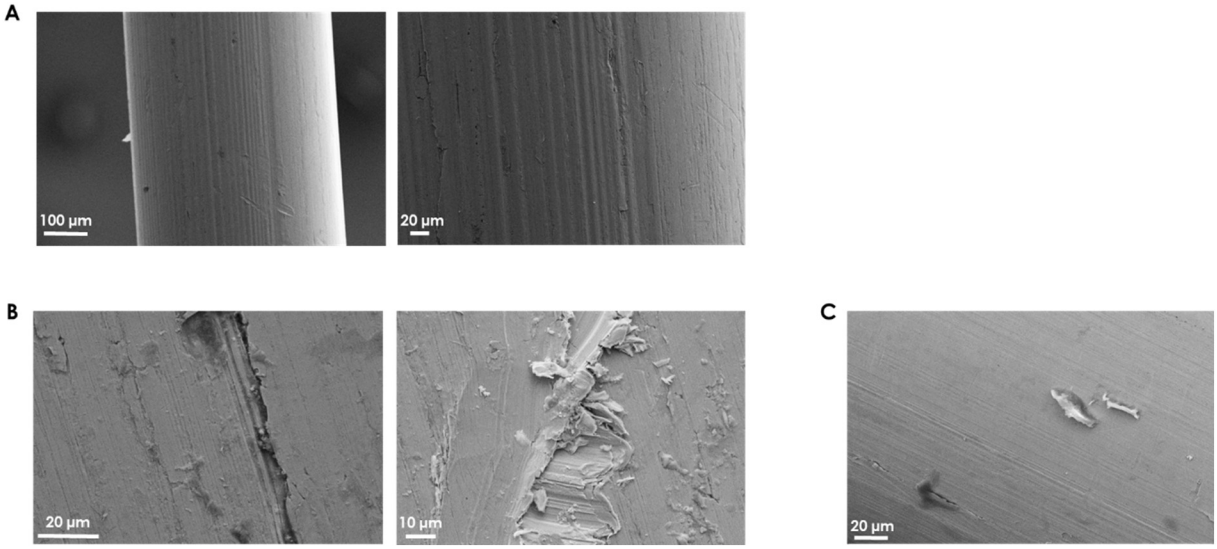

Fig. 2. Corrosion of Fe or 316L stainless steel wire samples. SEM analysis before or after corrosion in Tyrode solution for 6 h/37 °C. (A) Fe wire before corrosion, (B) Fe wire after corrosion, (C) 316L wire after corrosion.

during 6 h and then analyzed by SEM. The wire surface was subjected to corrosion as shown in Fig. 2(A, B). After degradation, the external layer of Fe showed a deep localized corrosion attack, contrary to the 316L surface that, as expected, remained intact (Fig. 2C).

As during this corrosion Fe is supposed to generate HO·, we evaluated its production via terephthalate fluorimetric analysis. Compared to the blank and the stainless steel material (Fig. 3), the Fe wire generated large amounts of HO·. The specificity of the TA measurement was verified by adding the antioxidant catalase, which completely inhibited the signal, consistent with the reaction in Fig. 1.

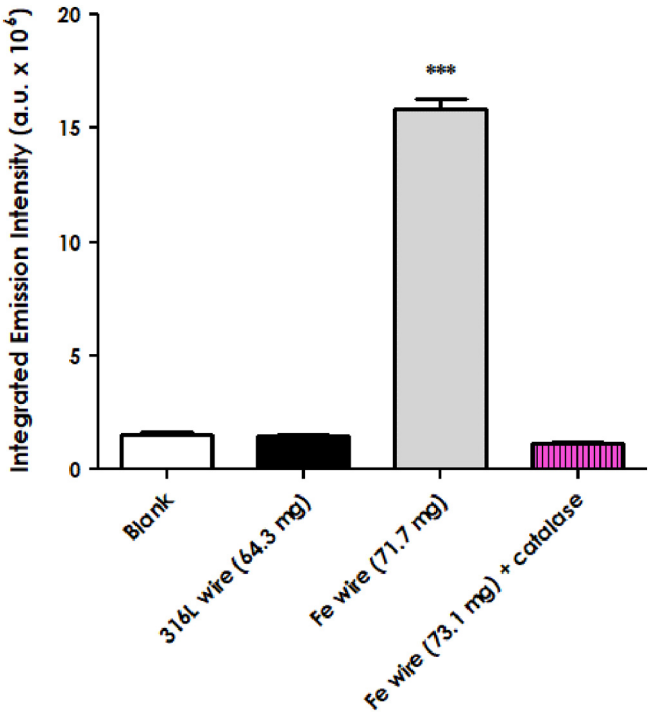

Fig. 3. The corrosion of Fe wire generates hydroxyl radicals. Fluorimetric determination of HO· released from Fe wire using the terephthalate (TA) assay. Samples were immersed in a buffered (PBS) solution of disodium terephthalate (10 mM) for 30 min at RT under continuous stirring in the absence/presence of catalase (1000 U/ml). Supernatant was recovered, filtered (0.22 µm) and fluorescence was measured (excitation λ_{ex} = 324 nm, emission λ_{em} = 425 nm). Values are means ± SEM (N = 2, n = 4).

The ability of the Fe wire to generate HO· presented here is consistent with our previous results in which HO· release by Fe-based materials was documented using a different readout, the EPR assay [7].

3.2. HO· released during Fe corrosion induce oxidative stress, decreased NO production by eNOS uncoupling, and endothelium dysfunction

A new *ex-vivo* model using Fe wire and aortic rings was developed to assess the influence of corrosion. We reasoned that short-lived HO· generated during corrosion can only exert their deleterious effects through intimate contact with cells. Hence, the implication of HO· was investigated with a direct contact test using a Fe wire inserted into an aortic ring. Addition of catalase or indirect exposure were used as controls. Preliminary experiments were conducted to determine an appropriate duration of exposure of the aortic rings to the Fe wire able to detect changes without affecting the viability of the rings. An incubation of 6 h was selected as appropriate (not shown). Great care was taken not to damage the endothelium by the insertion and/or removal of the wire, and the integrity of the endothelium after 6 h wire exposure was confirmed by immunofluorescence analysis (Fig. 4) which demonstrated an intact layer of VE-cadherin expressing endothelial cells after wire exposure and removal.

3.2.1. Oxidative stress response

We reasoned that if HO· affect arterial tissue during Fe corrosion, oxidative stress should be evident in cells exposed to Fe. It was, therefore, evaluated by monitoring the expression of nuclear factor erythroid 2-related factor (*Nrf2*) and heme oxygenase-1 (*HO-1*) in aortic rings. Both were increased after direct exposure to a Fe wire, whereas direct exposure to the stainless steel 316L wire did not induce such a response (Fig. 5A and Fig. S1). The expression of *Nrf2* and *HO-1* was not modified in the presence of catalase (Fig. 5B and Fig. S1) or after indirect exposure (Fig. 5B), consistent with the implication of HO· in the oxidative stress response.

3.2.2. NO production and eNOS signaling pathway

We next explored the impact of Fe corrosion and HO· on the production of NO by the endothelium. Ionomycin-stimulated NO production was measured by EPR spin trapping in isolated aortic rings after exposure to Fe or 316L wires. NO production was significantly decreased by the corrosion of Fe, but not with 316L (Fig. 6A, B) or in the

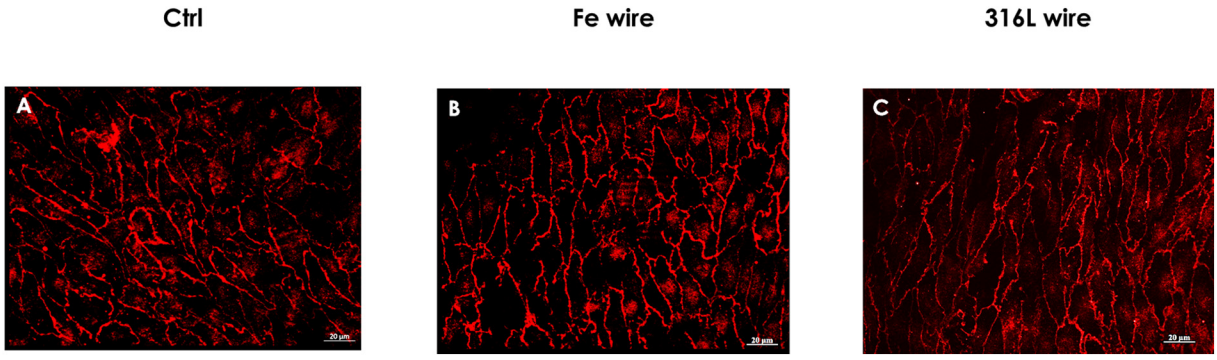

Fig. 4. Integrity of the endothelial layer after metal exposure. Aortic rings were dissected from Wistar rats and a metallic wire for 6 h. After removal of the wire, expression and localization of VE-cadherin was assessed by immunostaining of the full-thickness specimens and examination by ApoTome microscopy. Control aortic ring (A), Fe wire exposure (B) or 316L wire exposure (C). Magnification of 40×. The images are representative of 3 independent experiments.

presence of catalase (Fig. 6C).

Similar results were obtained when bovine aortic endothelial cells (BAECs) stimulated by calcium-ionophore were directly exposed to Fe (Fig. 7). Treatment of aortic rings or endothelial cells with a non-selective NOS inhibitor (L-NAME) reduced NO levels to baseline levels, supporting the specificity of the measurements.

In order to explain why NO production was affected, we evaluated the effect of HO· generated by the corrosion of Fe on eNOS activity in BAECs. It is well-established that oxidative stress can lead to uncoupling of eNOS and reduced NO production [20]. We therefore assayed the monomer/(monomer + dimer) ratio of eNOS proteins by Western blotting in BAECs instead of aortic rings which were less suitable for obtaining a sufficient amount of endothelial proteins. The monomer/(monomer + dimer) ratio increased by 63% over control in cells exposed to Fe, while the presence of catalase or 316L did not induce eNOS uncoupling (Fig. 8). These results suggested that eNOS uncoupling contributes to reduce NO production caused by HO· during Fe corrosion.

3.2.3. Vasodilatory dysfunction

Finally we investigated if all these effects, resulting from HO· generated during direct contact between the endothelium and Fe, affected endothelium function. The organ bath system is a valid method to investigate the physiology of isolated vessels, and an isometric measurement is most commonly used to measure vascular contractility as the vessel length remains constant. Fe or 316L exposure did not affect the amplitude of the contractile response to high KCl or Phe treatment (not shown, $p < 0.05$). A reduced carbachol-evoked relaxation after Fe exposure reflected an altered endothelium-dependent vasodilatatory profile as compared to controls or rings exposed to 316L (Fig. 9A). To dissect the implication of NO versus other endothelium-dependent components (namely, EDH(F) and PGI_2 alone), experiments were performed with eNOS and cyclooxygenase (COX) inhibitors. When vessels were preconstricted with a high KCl solution (to block EDH(F)) and incubated with a COX inhibitor (indomethacin, to block PGI_2 synthesis), the relaxation of rings exposed to Fe remained significantly altered (vs. control or 316L exposure), indicating an effect on NO-mediated relaxation (Fig. 9B). In contrast, when rings were preconstricted with Phe and incubated with NOS and COX inhibitors or preconstricted with a high KCl solution and incubated with a COX inhibitor, they were not affected in their Cch relaxation capacity (Fig. 9C, D). EDH(F) and PGI_2 alone are not operative in our conditions. Indeed, in conducting arteries such as aorta the EDH(F) is not present, and the formation of PGI_2 is mainly enhanced in pathological conditions, e.g. diabetes or atherosclerosis [14].

Direct contact with the material in the presence of catalase, or

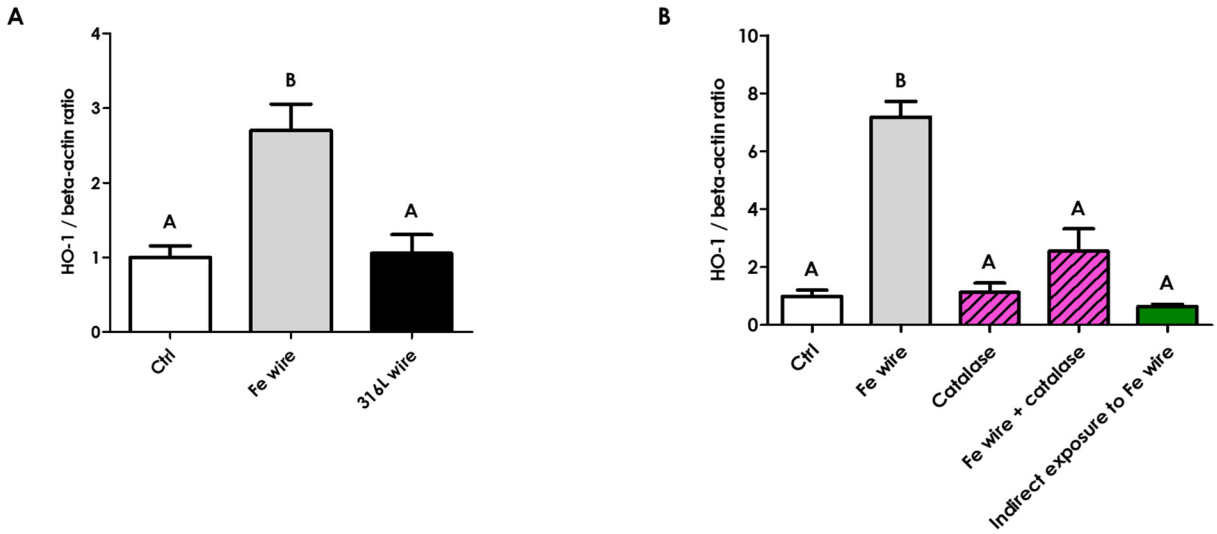

Fig. 5. Fe corrosion induces oxidative stress in aortic rings. Aortic rings were exposed directly to Fe wire in the absence/presence of catalase (1000 U/ml), 316L wire, or indirectly exposed to Fe wire for 6 h, at 37 °C. RNA was extracted and reverse transcribed for real-time polymerase chain reactions (RT-qPCR). Values of heme oxygenase-1 (*HO-1*) transcripts were normalized to *β-actin* amplified from the same sample and are presented as fold increase compared to untreated rings. Values are means ± SEM. (A) N = 7, (B) N = 2, (A, B), n = 2. Data with different superscript letters are significantly different at $p < 0.05$ (ANOVA followed by a post-hoc Tukey's test).

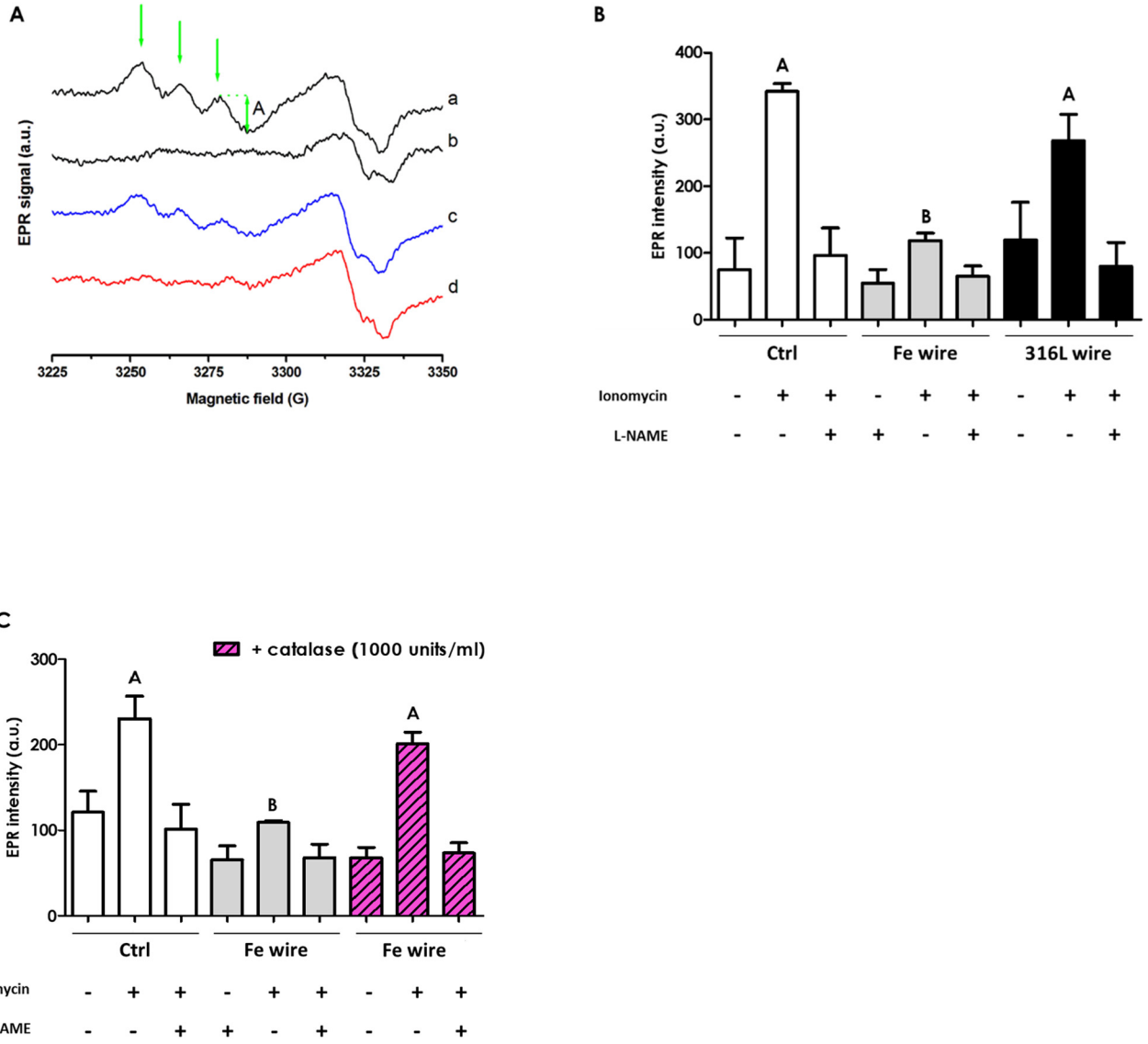

Fig. 6. The generation of HO· during Fe corrosion inhibits nitric oxide (NO) production by aortic rings. (A) Typical EPR spectra recorded in aortic rings after stimulation with 5 μM ionomycin alone (a) or with 2 mM L-NAME (b) or after exposure to 316L wire (+5 μM ionomycin, c) or Fe wire (+5 μM ionomycin, d). (B) Quantification of 3 independent experiments of aortic rings exposed to Fe or 316L wire (C) and to Fe wire in the presence/absence of catalase (1000 U/ml) at 37 °C for 6 h and then stimulated with 5 μM ionomycin. NO production was measured by electron paramagnetic resonance (EPR) spin trapping with the colloid complex [(diethyldithiocarbamate)$_2$Fe(II)] for 30 min. L-NAME (2 mM) was used as control to assess the specificity of the measurements. Values are means ± SEM. N = 3, n = 3. Data with different superscript letters are significantly different at $p < 0.05$ (ANOVA followed by a post-hoc Tukey's test).

indirect exposure did not affect relaxation, neither for the total endothelium-dependent relaxation (Fig. 10A, C), nor for the NO-mediated relaxation (Fig. 10B, D).

We concluded that Fe corrosion affected NO-mediated endothelium-dependent relaxation capacity in isolated aortic rings.

4. Discussion

Biodegradable metallic implants with temporary function have been proposed for cardio-vascular applications to overcome the disadvantages of permanent devices such as prolonged physical irritation, chronic inflammation and the need for prolonged anti-platelet aggregation therapy. As these temporary stents should remain in the artery for no > 6 and 12 months, the interplay between biodegradation and toxicity is a fundamental issue that should be carefully considered. Previous *in vivo* experiments on corrodible Fe stents implanted into the descending aorta of New Zealand white rabbits showed a slow degradation rate without signs of local or systemic toxicity [4]. Fe degradable stents were also implanted in porcine descending aorta. After 1-year, large portions of the stent were still intact and no signs of iron-overloading or iron-related toxicity were observed [21]. Fe stents were also implanted into the coronary arteries of juvenile domestic pigs and, after 28-days, no inflammation or fibrin deposition was recorded [22].

These previous investigations on bioresorbable Fe stents focused on local and systemic toxicity, Fe overload, thrombogenicity, inflammation and neointima proliferation in order to evaluate biocompatibility. Because a pure Fe stent is very light (~40 mg) and its degradation rate is slow (200 μg/day in 6 months), the Fe released from the stent is far less than the high Fe content in blood (447 mg/l). Therefore, the degradation products of Fe cannot cause systemic toxicity or Fe overload [23]. Moreover, no pronounced inflammation or thrombus formations or significant narrowing of the stented animal artery were evidenced. Based mainly on these observations, investigators came to the conclusion that stents made of biocorrodible Fe are safe and biocompatible.

Balloon angioplasty and stenting cause a complete to partial

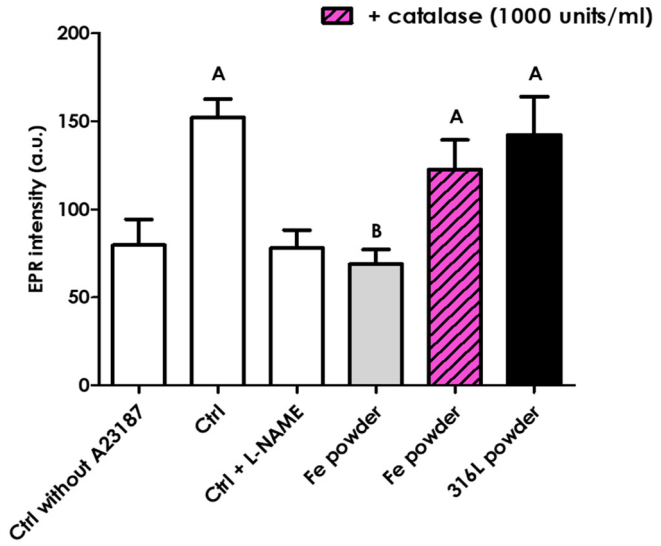

Fig. 7. Fe corrosion inhibits NO production by endothelial cells. Bovine aortic endothelial cells (BAECs) were exposed to Fe powder (100 μg/ml) with/without catalase (1000 U/ml) or 316L powder (100 μg/ml) for 24 h, and then stimulated with 2 μM of the Ca^{2+}-ionophore A23187. NO production was measured by electron paramagnetic resonance (EPR) spin trapping with the colloid complex [$(diethyldithiocarbamate)_2Fe(II)$] for 45 min. L-NAME (2.5 mM) was used as control to assess the specificity of the measurements. Values are means ± SEM. N = 4, n = 2. Data with different superscript letters are significantly different at $p < 0.05$ (ANOVA followed by a post-hoc Tukey's test).

endothelial denudation and, consequently, smooth muscle cells (SMCs) migrate and proliferate from the media and intima forming a neointima layer [24]. Then, the regeneration and regrowth of the denuded endothelium originates from the remaining endothelial cells and uninjured segments at the stent edges until the formation of a complete neoendothelium a few weeks after implantation [25]. Previous studies on drug-eluting stents (DES) in rabbits already underlined the importance of a functional endothelium [26]. Indeed, it was shown that regenerated endothelial cells were structurally and functionally abnormal. Based on these observations, it was expected that after stent placement the regenerated endothelium would be functionally incompetent. Moreover, stented vessels are usually affected by atherosclerosis and the endothelium of atherosclerotic vessels is dysfunctional a priori [15]. The preservation of a competently functional endothelium after stenting is critical for long-term vascular health [27]. Furthermore, an incompetent endothelium decreases the availability of NO, potentially leading to complications such as late stent thrombosis and the development of in-stent neoatherosclerosis [28].

The biocompatibility of metallic stents is mainly determined by their solubilisation and degradation products [23]. Degradation products not only include free metals ions, but also organic complexes and free radicals. This work mainly explored the impact of HO· produced during the corrosion of Fe-based materials on endothelial function. We found that HO· generated via a Fenton reaction induce oxidative stress and inhibit NO production which is an early manifestation of endothelium dysfunction through eNOS uncoupling, leading to reduced arterial relaxation capacity. The direct oxidation of tetrahydrobiopterin (BH_4) or increased S-glutathionylation could be possible mechanisms implicated in the eNOS uncoupling [29]. Uncoupled eNOS also generates superoxide ($O_2\cdot^-$) at the expense of NO, contributing further to endothelial dysfunction [30]. The implication of superoxide anion in the deleterious effects induced by Fe corrosion is further supported by previous *in vitro* experiments, in which pretreatment with superoxide dismutase-polyethylene glycol (PEG-SOD, 1000 U/ml, Sigma) fully protected ECs from Fe toxicity (*data not shown*).The focus is on the formation of HO·, the most deleterious ROS, specifically generated during the corrosion of Fe-based materials [31]. The implication of HO· was confirmed using the antioxidant catalase, which protected the endothelium from the deleterious impact of HO· by degrading hydrogen peroxide. The aim to perform indirect exposure assays was to support our working hypothesis, because in these tests the possible contribution of short-lived ROS was not possible, leaving only degradation products generated by the corrosion (e.g. Fe^{3+} ions). No effect of indirect exposure was observed in the different assays, indicating that Fe^{3+} ions do not significantly affect the endothelium. The implication of HO· in endothelium dysfunction was definitely confirmed by adding catalase, that was able to preserve the endothelium against the HO· effects. The experiments with the addition of catalase further confirmed that Fe ions do not contribute to the deleterious effects because the enzyme suppresses HO· but not the oxidation of Fe.

With the experimental model used in this paper, we were able to investigate the mechanism by which Fe corrosion induces endothelial dysfunction. Although the geometry of a wire is not the same as the

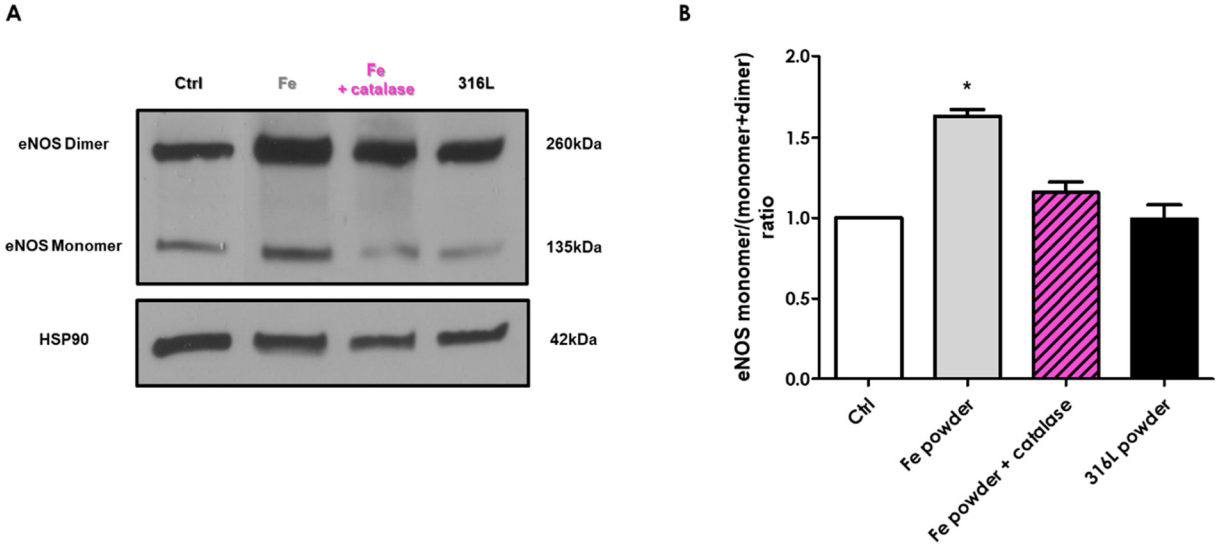

Fig. 8. HO· released from the corrosion of Fe induce eNOS uncoupling in endothelial cells. Bovine aortic endothelial cells (BAECs) were exposed to Fe powder (100 μg/ml) in the presence/absence of catalase (1000 U/ml) or 316L powder (100 μg/ml) for 24 h. (A) Representative eNOS immunoblotting signals from nondenatured EC lysates; (B) Densitometric analysis of eNOS monomer/(monomer + dimer) ratio. Values are means ± SEM. N = 3, n = 1.

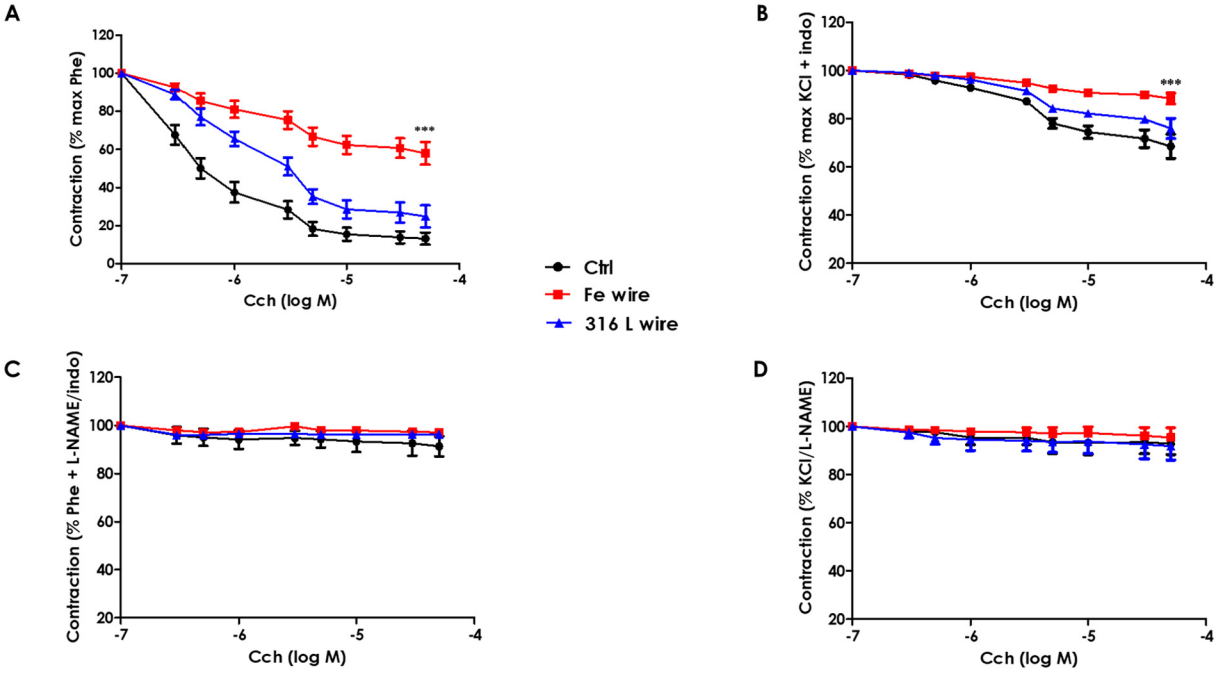

Fig. 9. Fe corrosion induces endothelial dysfunction in rat aorta rings. Carbachol (Cch) concentration-response curves of endothelium-intact aortic rings after exposure to Fe or 316L wire for 6 h, at 37 °C. Isolated relaxation pathways: (A) total relaxation was evaluated after contraction with phenylephrine (Phe, 3 μM). (B) NO-mediated relaxation was evaluated in the presence of indomethacin (indo, 10 μM) after contraction with high-KCl solution (100 mM). (C) EDH(F)-mediated relaxation was evaluated in presence of N-Ω-Nitro-L-arginine methyl ester (L-NAME, 100 μM) and indo (10 μM) after contraction with Phe (3 μM). (D) PGI2-dependent relaxation was assessed in presence of L-Ω-NoArg (100 μM) after KCl (100 mM) contraction. Values are means ± SEM. (A) N = 7, (B) N = 5, (C, D) N = 2; (A–D) n = 2. ***$p < 0.01$ vs ctrl (One-way ANOVA) at $10^{-4.3}$M Cch.

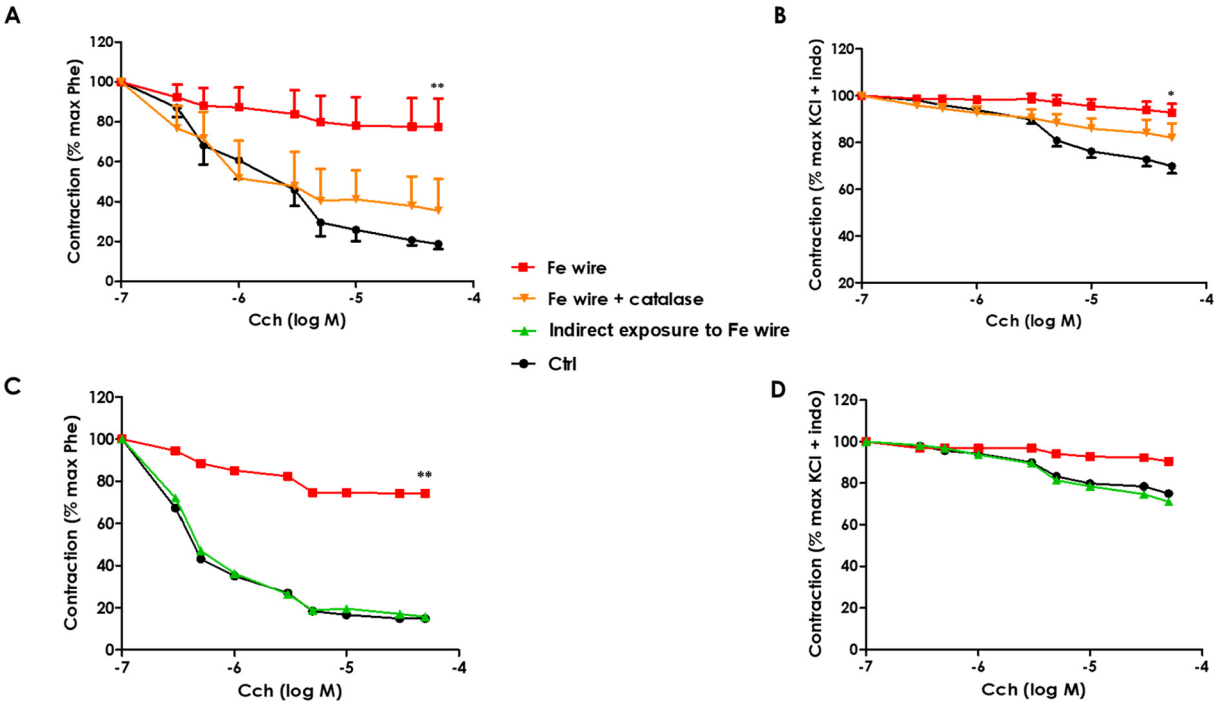

Fig. 10. The generation of HO· during Fe corrosion induces endothelial dysfunction in aortic rings. Effect of the combination of catalase (1000 U/ml) with direct contact to Fe wire or indirect exposure to Fe wire on carbachol-mediated relaxation in rat aortic rings. Vessels were exposed for 6 h, at 37 °C, prior to the evaluation of the total (A, C) or NO-mediated relaxation (B, D). Values are means ± SEM. (A, B) N = 5, (C, D) N = 2, (A-D) n = 2. **$p < 0.05$ vs ctrl (One-way ANOVA) at $10^{-4.3}$M Cch.

majority of commercial stents, a biodegradable metallic wire inserted into vessel rings provides a simple experimental model to investigate the impact of metal-based materials corrosion on the arterial wall.

As biocorrosion persists through the life of the implant, HO· are likely to be continuously formed and active at the implant site, worsening the local oxidative stress levels of the diseased tissue. Superoxide anions formed from uncoupled eNOS could exacerbate this oxidative stress, leading to a vicious circle. Superoxide can also avidly react with

vascular NO·, producing peroxynitrite ($ONOO^-$) which in turn leads to further damage [32]. These mechanisms can influence the success of the implantation, the healing and the function of arterial tissues and, ultimately, the stent degradation rate [5,33].

One of the potential limitations of this study concerns the use of healthy tissues while the target tissue, in humans, is by definition diseased when a stent is implanted. A diseased tissue is already submitted to oxidative stress [13], and it can be expected that the deleterious response is likely to be worse in an atheromatous tissue. Additional studies are also needed to examine the impact of Fe corrosion on SMCs which are in intimate contact with the stented implant.

5. Conclusion

The mechanisms highlighted here provide new information on the impact of biodegradable Fe-based implants on surrounding tissues. Until now, little was known about biomaterials and oxidative stress, and the mechanism underlying metal toxicity is still not fully understood [12]. We developed a simple model in which the endothelium was directly exposed by inserting a Fe wire into the lumen to mimic the endothelium-stent contact.

With this experimental design we showed that HO· released during Fe corrosion have a deleterious impact on endothelium, causing oxidative stress and an inhibition of NO production through a decreased eNOS enzymatic activity. This model can be valuable for understanding the impact of biodegradable Fe-based materials on arterial wall and may act as a point of reference for similar studies in other systems. Our findings contribute to raise concerns about the biocompatibility of degradable Fe-based alloys for vascular implants.

Supplementary data to this article can be found online at https://doi.org/10.1016/j.msec.2020.110938.

CRediT authorship contribution statement

E. Scarcello:Conceptualization, Methodology, Writing - original draft, Writing - review & editing.**I. Lobysheva**:Investigation.**C. Bouzin**:Methodology.**P.J. Jacques**:Funding acquisition.**D. Lison**:Conceptualization, Supervision, Writing - original draft, Writing - review & editing.**C. Dessy**:Supervision, Writing - original draft, Writing - review & editing.

Declaration of competing interest

The authors declare that they have no known competing financial interests or personal relationships that could have appeared to influence the work reported in this paper.

Acknowledgments

Funding: This work was supported by the “Communauté française de Belgique. Sections de Recherche Concertées” [contract 15/20-066] (principal promoter Pascal J. JACQUES). CD is a senior research associate of the FRS-FNRS.

References

[1] M. Moravej, D. Mantovani, Biodegradable metals for cardiovascular stent application: interests and new opportunities, Int. J. Mol. Sci. 12 (2011) 4250–4270, https://doi.org/10.3390/ijms12074250.
[2] A. Francis, Y. Yang, S. Virtanen, A.R. Boccaccini, Iron and iron-based alloys for temporary cardiovascular applications, J. Mater. Sci. Mater. Med. 26 (3) (2015) 138, https://doi.org/10.1007/s10856-015-5473-8.
[3] B. Heublein, R. Rohde, V. Kaese, M. Niemeyer, W. Hartung, A. Haverich, Biocorrosion of magnesium alloys: a new principle in cardiovascular implant technology? Heart J. 89 (2003) 651–656, https://doi.org/10.1136/heart.89.6.651.
[4] M. Peuster, P. Wohlsein, M. Brügmann, M. Ehlerding, K. Seidler, C. Fink, H. Brauer, A. Fischer, G. Hausdorf, A novel approach to temporary stenting: degradable cardiovascular stents produced from corrodible metal—results 6–18 months after implantation into New Zealand white rabbits, Heart (London, U. K.) 86 (2001) 563–569, https://doi.org/10.1136/heart.86.5.563.
[5] J.L. Gilbert, G.W. Kubacki, Chapter three - oxidative stress, inflammation, and the corrosion of metallic biomaterials: corrosion causes biology and biology causes corrosion, in: Dziubla, Butterfield (Eds.), Oxidative Stress and Biomaterials, Academic Press, 2016, pp. 59–88.
[6] H.J. Lee, H. Lee, H.E. Kim, J. Kweon, B.D. Lee, C. Lee, Oxidant production from corrosion of nano- and microparticulate zero-valent iron in the presence of oxygen: a comparative study, J. Hazard. Mater. 265 (2014) 201–207, https://doi.org/10.1016/j.jhazmat.2013.11.066.
[7] E. Scarcello, A. Herpain, M. Tomatis, F. Turci, P.J. Jacques, D. Lison, Hydroxyl radicals and oxidative stress: the dark side of Fe corrosion, Colloids Surf B: Biointerfaces B 185 (2020), https://doi.org/10.1016/j.colsurfb.2019.110542.
[8] H. Ahsan, A. Ali, R. Ali, Oxygen free radicals and systemic autoimmunity, Clin. Exp. Immunol. 131 (2003) 398–404, https://doi.org/10.1046/j.1365-2249.2003.02104.x.
[9] M.B. Hampton, A.J. Kettle, C.C. Winterbourn, Inside the neutrophil phagosome: oxidants, myeloperoxidase, and bacterial killing, Blood 92 (9) (1998) 3007–3017.
[10] M. Peuster, C. Henne, T. Schloo, C. Fink, P. Beerbaum, C. von Schnakenburg, Long-term biocompatibility of a corrodible peripheral iron stent in the porcine descending aorta, Biomaterials 27 (28) (2006) 4955–4962, https://doi.org/10.1016/j.biomaterials.2006.05.029.
[11] D. Lison, P. Carbonnelle, L. Mollo, R. Lauwerys, B. Fubini, Physicochemical mechanism of the interaction between cobalt metal and carbide particles to generate toxic activated oxygen species, Chem. Res. Toxicol. 8 (4) (1995) 600–606, https://doi.org/10.1021/tx00046a015.
[12] P.A. Mouthuy, S.J.B. Snelling, S.G. Dakin, L. Milkovic, A.C. Gasparovic, A.J. Carr, N. Zarkovic, Biocompatibility of implantable materials: an oxidative stress viewpoint, Biomaterials 109 (2016) 55–68, https://doi.org/10.1016/j.biomaterials.2016.09.010.
[13] K. Chen, J.F. Keaney Jr., Evolving concepts of oxidative stress and reactive oxygen species in cardiovascular disease, Curr. Atheroscler. Rep. 14 (5) (2012) 476–483, https://doi.org/10.1007/s11883-012-0266-8.
[14] M. Romero, E. Leon-Gomez, I. Lobysheva, G. Rath, J.M. Dogne, O. Feron, C. Dessy, Effects of BM-573 on endothelial dependent relaxation and increased blood pressure at early stages of atherosclerosis, PLoS One 11 (3) (2016) e0152579, , https://doi.org/10.1371/journal.pone.0152579.
[15] A. Cornelissen, F.J. Vogt, The effects of stenting on coronary endothelium from a molecular biological view: time for improvement? J. Cell. Mol. Med. 23 (1) (2019) 39–46, https://doi.org/10.1111/jcmm.13936.
[16] S.P. Duckles, V.M. Miller, Hormonal modulation of endothelial NO production, Pflugers Arch. 459 (6) (2010) 841–851, https://doi.org/10.1007/s00424-010-0797-1.
[17] W. Wallace, L.A. Taylor, Y. Liu, B.L. Cooper, D.S. McKay, B. Chen, A.S. Jeevarajan, Lunar dust and lunar simulant activation and monitoring, Meteorit. Planet. Sci. 44 (7) (2009) 961–970, https://doi.org/10.1111/j.1945-5100.2009.tb00781.x.
[18] F. Rouaud, M. Romero-Perez, H. Wang, I. Lobysheva, B. Ramassamy, E. Henry, P. Tauc, D. Giacchero, J.L. Boucher, E. Deprez, S. Rocchi, A. Slama-Schwok, Regulation of NADPH-dependent nitric oxide and reactive oxygen species signalling in endothelial and melanoma cells by a photoactive NADPH analogue, Oncotarget 5 (2014), https://doi.org/10.18632/oncotarget.2525.
[19] I. Lobysheva, G. Rath, B. Sekkali, C. Bouzin, O. Feron, B. Gallez, C. Dessy, J.L. Balligand, Moderate caveolin-1 downregulation prevents NADPH oxidase-dependent endothelial nitric oxide synthase uncoupling by angiotensin II in endothelial cells, Arterioscler. Thromb. Vasc. Biol. 31 (9) (2011) 2098–2105, https://doi.org/10.1161/ATVBAHA.111.230623.
[20] S. Batova, J. DeWever, T. Godfraind, J.L. Balligand, C. Dessy, O. Feron, The calcium channel blocker amlodipine promotes the unclamping of eNOS from caveolin in endothelial cells, Cardiovasc. Res. 71 (3) (2006) 478–485, https://doi.org/10.1016/j.cardiores.2006.04.013.
[21] M. Peuster, C. Hesse, T. Schloo, C. Fink, P. Beerbaum, C. von Schnakenburg, Long-term biocompatibility of a corrodible peripheral iron stent in the porcine descending aorta, Biomaterials 27 (2006) 4955–4962, https://doi.org/10.1016/j.biomaterials.2006.05.029.
[22] R. Waksman, R. Pakala, R. Baffour, R. Seabron, D. Hellinga, F.O. Tio, Short-term effects of biocorrodible iron stents in porcine coronary arteries, J. Interv. Cardiol. 21 (1) (2008) 15–20, https://doi.org/10.1111/j.1540-8183.2007.00319.x.
[23] T. Hu, C. Yang, S. Lin, Y. Qingsong, G. Wang, Biodegradable stents for coronary artery disease treatment: recent advances and future perspectives, Mater. Sci. Eng. C 91 (2018) 163–178, https://doi.org/10.1016/j.msec.2018.04.100.
[24] C. Chaabane, F. Otsuka, R. Virmani, M.L. Bochaton-Piallat, Biological responses in stented arteries, Cardiovasc. Res. 99 (2) (2013) 353–363, https://doi.org/10.1093/cvr/cvt115.
[25] P.H. Grewe, T. Deneke, A. Machraoui, J. Barmeyer, K.M. Müller, Acute and chronic tissue response to coronary stent implantation: pathologic findings in human specimen, J. Am. Coll. Cardiol. 35 (1) (2000), https://doi.org/10.1016/S0735-1097(99)00486-6.
[26] J.A. Leopold, Neoatherosclerosis: another consequence of endothelial dysfunction? Circ. Cardiovasc. Interv. 7 (5) (2014) 635–637, https://doi.org/10.1161/CIRCINTERVENTIONS.
[27] F. Otsuka, A.V. Finn, S.K. Yazdani, M. Nakano, F.D. Kolodgie, R. Virmani, The importance of the endothelium in atherothrombosis and coronary stenting, Nat. Rev. Cardiol. 9 (2012) 439, https://doi.org/10.1038/nrcardio.2012.64.
[28] T. Gori, Endothelial function: A short guide for the interventional cardiologist, Int. J. Mol. Sci. 19 (12) (2018), https://doi.org/10.3390/ijms19123838.
[29] J.L. Zweier, C.A. Chen, L.J. Druhan, S-Glutathionylation Reshapes Our

Understanding of Endothelial Nitric Oxide Synthase Uncoupling and Nitric Oxide/Reactive Oxygen Species-Mediated Signaling. Antioxid Redox Signal 14 (10) (2011) 1769–1775, https://doi.org/10.1089/ars.2011.3904.
[30] H. Shimokawa, T. Matoba, Hydrogen peroxide as an endothelium-derived hyperpolarizing factor, Pharmacol. Res. 49 (6) (2004) 543–549, https://doi.org/10.1016/j.phrs.2003.10.016.
[31] T. Dziubla, D. Allan Butterfield, Oxidative Stress and Biomaterials, Elsevier book, 2016.
[32] U. Forstermann, T. Munzel, Endothelial nitric oxide synthase in vascular disease: from marvel to menace, Circulation 113 (13) (2006) 1708–1714, https://doi.org/10.1161/CIRCULATIONAHA.105.602532.
[33] R. Tsaryk, M. Kalbacova, U. Hempel, D. Scharnweber, R.E. Unger, P. Dieter, C.J. Kirkpatrick, K. Peters, Response of human endothelial cells to oxidative stress on Ti6Al4V alloy, Biomaterials 28 (2007) 806–813, https://doi.org/10.1016/j.biomaterials.2006.09.033.